Elsevier Editorial System(tm) for Advanced Powder Technology

Manuscript Draft

Manuscript Number: APT-D-18-00999R1

Title: Plasmon enhanced luminescence in hierarchically structured Ag@ (Y0.95Eu0.05)2O3 nanocomposites synthesized by ultrasonic spray pyrolysis

Article Type: Original Research Paper

Keywords: rare earth elements, ultrasonic spray pyrolysis, photoluminescence, plasmon

Corresponding Author: Miss Gözde Alkan,

Corresponding Author's Institution: RWTH Aachen

First Author: Gözde Alkan

Order of Authors: Gözde Alkan; Lidija Mancic; Sayaka Tamura; Koji Tamuta; Zhenquan Tan; Feifei Sun; Rebeka Rudolf; Satoshi Ohara; Bernd Friedrich; Olivera Milosevic

Abstract: Ag@ (Y0.95 Eu0.05)2O3 nanocomposites were synthesized by single step Ultrasonic Spray Pyrolysis (USP). 800 °C synthesis temperature and 1.5 l/ min air flow were determined as optimal USP parameters. A detailed parametric study was conducted on samples with varying silver content and heat treatment conditions. The effect of silver in both as prepared and heat treated samples were elucidated in terms of structural and functional properties. Ag incorporation decreased luminescence efficiency due to the lack of crystallization of matrix and non-homogenous distribution of Eu and Ag in as prepared samples. Heat treatment improved luminescence by improved crystal quality for all samples; however, with increasing Ag content effect of heat treatment was more pronounced owing to uniform distribution of Ag. 2.5 wt. % Ag addition followed by 2 hours heat treatment after USP synthesis is suggested as the most efficient nanocomposite for red light emitting down converting phosphor applications.

***Graphical Abstract (for review)**

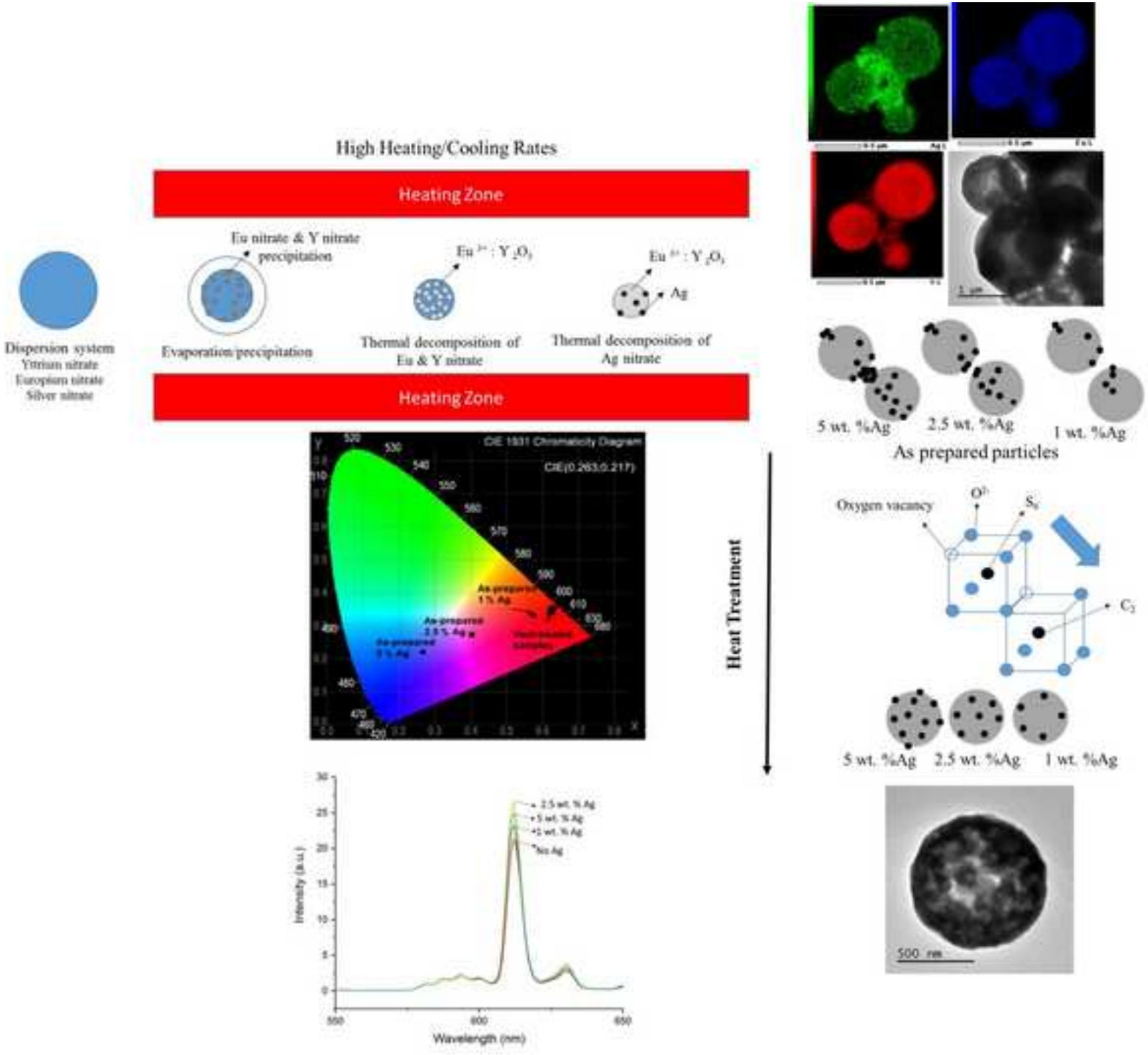

***Highlights (for review)**

- Down converting Ag@ $(Y_{0.95}Eu_{0.05})_2O_3$ were successfully synthesized by one-step ultrasonic spray pyrolysis.
- Effect of Ag incorporation and heat treatment on photoluminescence efficiency were elucidated.
- Heat treated samples exhibited enhanced luminescence with Ag incorporation.
- All heat treated samples exhibited red light emitting close to ideal red chromacity (0.67, 0.33).

Plasmon enhanced luminescence in hierarchically structured Ag@ $(Y_{0.95}Eu_{0.05})_2O_3$ nanocomposites synthesized by ultrasonic spray pyrolysis

Gözde Alkan[1], Lidija Mancic[2], Sayaka Tamura[3], Koji Tomita[3], Zhenquan Tan[4], Feifei Sun[4], Rebeka Rudolf[5], Satoshi Ohara[6], Bernd Friedrich[1], Olivera Milosevic[2]

[1]RWTH, Aachen University, Aachen, Germany

[2]Institute of Technical Sciences of Serbian Academy of Sciences and Arts, K.Mihajlova 35, 11000 Belgrade, Serbia

[3]Tokai University, Japan

[4] Dalian University of Technology, China.

[5] Univeristy of Maribor, Slovenia

[6]JWRI, Osaka University, Osaka, Japan

Abstract

Ag@ $(Y_{0.95}Eu_{0.05})_2O_3$ nanocomposites were synthesized by single step Ultrasonic Spray Pyrolysis (USP). 800 °C synthesis temperature and 1.5 l/ min air flow were determined as optimal USP parameters. A detailed parametric study was conducted on samples with varying silver contents and heat treatment conditions. The effect of silver in both as prepared and heat treated samples were elucidated in terms of structural and functional properties. Ag incorporation decreased luminescence efficiency due to the lack of crystallization of matrix and non-homogenous distribution of Eu and Ag in as prepared samples. Heat treatment improved luminescence by improved crystal quality for all samples; however, with increasing Ag content effect of heat treatment was more pronounced owing to uniform distribution of Ag. 2.5 wt. % Ag addition followed by 2 hours heat treatment after USP synthesis is suggested as the most efficient nanocomposite for red light emitting down converting phosphor applications.

Keywords: noble metals, rare earth elements, doping, ultrasonic spray pyrolysis, photoluminescence, plasmon

1. Introduction

Europium (Eu^{3+}) doped yttrium oxide (Y_2O_3) has been the focus of many studies as a photoluminescent (PL) material owing to high quantum efficiency, large band gap (5.8 eV), low phonon energy (430-550 cm^{-1}), tunable

emission wavelength, similar atomic radii of Y^{3+} and Eu^{3+} which favors atomic replacement [1]. Moreover, their together use exhibits sharper emission lines due to the outer less energetic 5s and 5p shells that protect the f electrons from external forces of Eu^{3+} and suppresses resonant energy transfer that provides high-concentration luminescence [2]. Further enhancement is not possible through increasing rare earth (RE) ions due to the concentration quenching effect and the optimal doping ratio is reported as 4-6 at. % in previous studies [3-5].

An alternative strategy is the surface plasmon enhancement of luminescence by incorporating metallic nanoparticles to phosphor materials [6-10]. There have been many studies conducted on Eu complex solutions including silver, and the effect of Ag nanoparticles on PL efficiency were investigated [11-15]. Generally, two mechanisms were reported for the enhancement of luminescence; energy transfer (ET) between Eu and Ag and local electromagnetic field enhancement (LFE); respectively. When an off-resonance excitation is used, where Ag cannot absorb the light, surface plasmons of Ag provide a confined electromagnetic field around emitting rare earth ions, and therefore increased emission efficiencies are reported [12,13]. In another study conducted by G. Kaur et al., with an excitation wavelength of 400 nm, absorption of light by Ag and transfer of this excitation energy to lanthanide ions were reported, that enhances emission efficiency [16]. All studies, in a parallel manner, reported a critical Ag concentration that enhances luminescence efficiency but after that result in emission quenching. Quenching effect was due to absorption competition between Ag and Eu^{3+}, re-absorption of emitted light by metal nanoparticles and energy transfer from Eu^{3+} to Ag, when Ag concentration increases and distance between metal particles and to emitter ion decrease [12, 13]. Although there have been promising results achieved in solution and dispersion phases of Eu complexes in the presence of Ag, in solid phase where interaction between constituents differ from the case in solution, there are only a few studies available in literature. Ferrari et al. elucidated $Ag@Y_2O_3$:Eu (5 at. %) system in terms of effect of Ag on luminescence efficiency and reported a slight increase owing to metal enhanced crystallization of matrix [17]. Similarly, Rabanal et al. investigated $Ag@Y_2O_3$:Eu (9 at. %) nanocomposites synthesized by ultrasonic spray pyrolysis (USP) and reported enhancement at lower Ag concentrations and worsening at higher Ag concentration [18].

Since ET and LFE strongly depend on the particle size, distribution, emitter concentration, host matrix, we aimed a systematic parametric and comparative study on $Ag@Y_2O_3$:Eu hierarchical nanocomposites synthesized by USP. Through USP process, the starting ultrafine droplets act as a micro-reactor and ensures formation of fine

particles. Moreover, since the mix of all constituents are atomized and experience reaction together in this defined volume, the formation of uniform hierarchic structures are favored as reported in previous studies [1,8, 18]. USP process temperature, Ag concentration and heat treatment conditions were examined for the highest red-phosphor emission efficiency. Structural characterization techniques such as Scanning Conventional and High resolution Transmission Electron Microscopy (SEM, CTEM, HRTEM) coupled with energy dispersive x-ray analysis , x-ray powder diffraction (XRPD) analysis using Rietveld refinement and EPMA (Electron Probe Microanalyse) had been utilized to reveal the morphology and crystal structure, distribution of the constituents, and interaction between metallic silver and Eu: Y_2O_3. These microstructural properties were utilized to explain differences between PL efficiencies of samples and the most efficient process conditions was proposed.

2. Experimental Procedure

Yttrium nitrate ($Y(NO_3)_3.6H_2O$, Aldrich, purity > 99 %), europium nitrate ($Eu(NO_3)_3{\cdot}5H_2O$, Aldrich, purity > 99 %) and silver nitrate ($AgNO_3$, AppliChem, purity > 98 %) commercial precursors were used as yttrium oxide, europium, and silver precursors, respectively. De-ionized water was used for all solutions as the solvent**.** In a typical synthesis, the precursor solutions were prepared with dissolving the relative amounts of $Y(NO_3)_3.6H_2O$, $Eu(NO_3)_3{\cdot}5H_2O$ and $AgNO_3$ in de-ionized water to be used in classical ultrasonic spray pyrolysis (USP) with main parts of ultrasound generator (1.7 MHz, Gapusol, RBI, France), a carrier gas (air) inlet connected over a flow regulator (1.5 l/min), horizontal wall heated furnace with quartz tube and washing bottles for collection purposes. Details of this experimental setup can be found elsewhere [18]. All precursors are atomized together and carried by air to heating zone, set at target temperature previously to experience evaporation, precipitation and thermal decomposition together. Some selected samples were exposed to post heat treatment at 1000 °C in an inert argon ambient to prevent the oxidation of silver. Detailed experimental plan is listed in Table 1, where various silver concentrations (0 wt. %, 1wt. %, 2.5wt. %, 5 wt. %, 7.5 wt. % and 10 wt. %), USP temperatures (800°C, 900°C, 1000 °C) and heat treatment conditions (no heat treatment, 2 h, 12 h) were studied. For all samples 5 at.% Eu was kept constant considering a previous study indication the optimal Eu doping is between 4-6 at. % [3]. Since same gas flow rate, temperature and reactor were used, estimated residence time is 3.3 s for all samples.

	Ag concentration (wt.%)	USP Temperature (°C)	Subsequent Heat Treatment Time (h)
ref*	-	800	-
ref*	-	800	2
ref*	-	800	12
*	1	800	-
*	1	800	2
*	1	800	12
*	2.5	800	-
*	2.5	800	2
*	2.5	800	12
*	5	800	-
*	5	800	2
*	5	800	12
	5	900	-
	5	1000	-
	7.5	800	-
	10	800	-

Table 1. Synthesis conditions of Ag@$(Y_{0.95}Eu_{0.05})_2O_3$nanocomposites

(ref) Samples without silver for direct comparison purpose *samples analysed in terms of photoluminescence efficiency

The crystal structure and phase content of synthesized powders were elucidated by means X-Ray Powder Diffraction (XRD) (Rigaku Ultima IV, 40kV/40mA).The patterns were recorded from 10 to 80° with a step scan of 0.02°and accounting time of 5 s per step.Powders structural data were acquired through Rietveld refinement in Topas 4.2. Software. FWHM based calculations were utilized to determine the average crystal size and strain values.

Morphological features of samples were analysed by scanning electron microscopy (SEM) Microscope JEOL, JSM T 330 and the chemical composition of the samples was determined using a Jeol JED-2300 Series energy dispersive spectrometer (EDS). Detailed microstructural analyses were conducted by conventional transmission electron microscopy using a Jeol JEM-2100 microscope operated at 200 kV accelerating voltage. Energy Dispersive X-ray Spectroscopy (EDS, JEOL JED-2300 Series) was used to examine the elemental composition of the specimens. Diluted colloid samples were dropped onto Cu-grids and the solvent was allowed to dry at room temperature. Analyses were performed at standard conditions; acquisition method- high resolution, live time mode, acquisition time 100s. High resolution Transmission electron microscopy (HRTEM) FEI Tecnai G2F30 was also used to monitor samples in atomic resolution. HRTEM images were collected by dropping the dispersion of powder sample onto a Cu grid and then dried in air before it was send into the FEI TEM operating at 200 kV accelerating voltage.In addition, Gatan Digital MicrographTM software was used to perform Fast Fourier Transformation (FFT) of the high resolution transmission electron microscopy images (HRTEM) and confirmation of the crystal structure.

The photoluminescence spectra of the particles were recorded at room temperature by the FP-8600 (JASCO) with a scan rate of 200 nm/min using a 150 W xenon lamp as an excitation source. Emmission spectra of each sample between 400-700 nm for the excitation wavelength between 200-400 nm were recorded Moreover, excitation spectra were analyzed by fitting the spectrum to three peaks centered at 210, 230 and 250 nm to reveal the energy transfer between excited Eu^{3+} ions in C_2 and S_6 positions.

3. Results and Discussion

3.1. Detailed microstructural and crystallographic study on as- prepared nanocomposites

SEM micrographs of nanocomposites with 5 wt. % Ag incorporation but synthesized at different temperatures , 800 °C, 900°C and 1000°C, can be seen in Fig 1 a, b and c; respectively to observe the synthesis temperature effect on microstructure.

Figure 1. Scanning Electron Microscopy images of USP products synthesized at **a**- 800°C, **b**-900 °C, **c**- 1000 °C

Almost dense and well-shaped spherical morphology of powders achieved by 800 °C represented in Fig 1a.With increasing reaction temperatures to 900 and 1000 °C, porous surfaces and exploded particles were appeared as shown in Fig 1 b and c. This may be due to increased evaporation rates as reported previously [19] and/or shorter residence times with increasing temperature, which would yield in deviation from equilibrium morphology. Therefore, 800 °C was selected as optimal USP process temperature and utilized in the rest of experiments.

In order to reveal the importance of Ag amount, varying silver concentration in the initial solution; 1 wt. %, 2.5 %, 5 %, 7.5 % and 10 % Ag were examined. Corresponding TEM micrographs can be found in Figure 2.

Figure 2. LRTEM images and corresponding EDX analyses of as-prepared nanocomposites with **a-** 1 **b-** 2.5 **c-**5 **d-** 7.5 **e-** 10 wt. % Ag

All samples exhibited the typical spherical morphology of USP independent from Ag concentration, where secondary particles represent an assemblage of primary nanoparticles around 20- 30 nm. LRTEM images also reveal that there is not a significant change in spherical shape of the particles with increased silver content and as reported previously, some porosities may be due to fast heating rates of process [18].EDX analyses performed on points indicated by arrows proves the presence of silver (Lα line at 2.98 kev) and also homogenous Eu (Lα line at 5.9 kev) and Y (Kα line at 14.9334 kev and Lα line at 1.9226 kev) and oxygen (K α line at 0.53 kev) distribution, Cu lines are due to copper grid used for TEM analyses. These analyses proved the presence of Ag within the volume of secondary particles for all samples, where it uses already existing primary crystal surfaces of Y_2O_3: Eu. However; higher silver concentrations resulted in appearance of very fine particles, which were revealed by EDX analyses as Ag or Ag enriched regions. Higher magnification inset in Fig 2b revealing hexagonal Ag precipitated onto secondary particle surface. Smooth morphology of that Ag nanoparticle implies the formation of Ag takes place from melt phase. In addition to those Ag located inside, with increasing Ag concentration, precipitation of silver at the surface was detected. Especially 7.5 and 10 wt. % Ag concentrations yielded in agglomerated fine Ag nanoparticles at the surface and connects Y_2O_3 particles together, which would decrease the specific surface area and may be detrimental to PCA. A more detailed analyses was performed on sample with 7.5 wt. %, in order to investigate the distribution of components through particles by EDX mapping as given in Figure 3.

Figure 3. EDS elemental mapping: overlay of silver, europium and yttrium to the sample

Figure 3 reveals that relatively bigger (secondary) particles (~500 nm) includes uniformly distributed of yttrium and europium elements. On the contrary, relatively fine silver nanoparticles (20-30 nm) are present rarely on the surface of bigger particles but mainly separately agglomerated, as detected also in TEM micrographs in Fig 2. Since agglomeration of silver nanoparticles are not favored in terms of photoluminescence efficiency, Ag composition higher than 5 wt. % is not promising. Therefore; more detailed structural and functional investigation was performed on three promising nanocomposites with 1, 2.5 and 5 wt. % Ag.

Figure 4 reveals XRD diffraction patterns of as- prepared (a.p.) powders with varying silver amount, plane ($(Y_{0.95}Eu_{0.05})_2 O_3$) is also given in the spectra for direct comparison purposes.

Figure 4. XRD diffraction patterns of (a) as- prepared powders with various silver content (b)Rietveld refinement of sample with 1 wt. % Ag

As it can be observed in Fig 4a, independent from various Ag content, all samples exhibit BCC cubic structure of $(Y_{0.95}Eu_{0.05})_2 O_3$ with space group la-3 according to JCPDS card 43-1036 [20]. However, peak broadenings imply poor crystal quality for all samples. It is also worth to emphasize that even within highest Ag including sample, there has not been any additional diffraction peak corresponding to Ag phase detected. This may be due to relatively short reaction times of USP, which do not allow Ag to well crystallized and incorporated to metal oxide based system. However, in the samples with Ag incorporation, there has been a slight increase observed in diffraction peak intensities that has been also previously reported by Ferrari et al. and explained as metal-induced crystallization effect [17,21]. Eu_2O_3 was also not detected in any XRD spectra, implying Eu (0.947 Å) replaces Y ions (0.90 °A). Moreover, there has not been any change in the unit cell parameter was observed with Ag incorporation, which implies Ag does not locate to the Y_2O_3 crystal structure. Refined crystallographic data for as- prepared samples in Table 2 revealed, as consistent with previous reports, a slight increase lattice parameter of

samples with respect to that of Y_2O_3(a:10.60 Å). It is due to slightly larger ionic radius of Eu^{3+}(0.95 Å) which replaces Y^{3+} (0.90 Å).

Table 2. Refined structural parameters of as- prepared nanocomposites

	No Ag (ap)	**1 wt. % Ag (ap)**	**2.5 wt. % Ag (ap)**	**5 wt. % Ag (ap)**
Unit cell parameter *a* (Å)	10.6302(7)	10.6292(5)	10.6257(6)	10.6248(5)
Crystallite size (nm)	14.1 (2)	15.9 (2)	15.6(2)	16.5(3)
OccY1 (C2)*	0.933	0.933	0.947	0.969
OccY2 (S6)*	0.981	0.981	0.939	0.873
R_{Bragg}	1.37	1.083	1.671	1.962
GoF	1.20	1.178	1.280	1.266
Rwp	7	6.566	7.038	7.884
Strain	0.301(8)	0.287(6)	0.237(8)	0.265(6)
Y1:O	2.1755(79)	2.1673(76)	2.1992(82)	2.2101(76)
Y2:O	2.3037(80)	2.3423(80)	2.3291(84)	2.3141(77)

Table 2 points out that, there was not any dramatic change in crystal size of samples (around 14-15 nm) with varying silver content observed. Although crystal size and XRD diffractions have not significantly affected by Ag, occupations of two nonequivalent crystallographic sites of Y^{3+} ions, a non-centrosymmetric C_2 and centrosymmetric S_6 exhibited variation with increasing Ag content. Where 1 corresponds to full site occupations of Y^{3+}, 1-OccY1 and 1-OccY2 values reveal the occupancy of Eu^{3+} in C_2 and S_6 sites; respectively. Especially with 2.5 and 5 wt. % Ag addition, Eu^{3+} is positioned more favorably in S_6 sites; revealing Ag incorporation modifies the neighborhood local symmetry of Eu^{3+} ions.

HRTEM images with FFT calculations in a comparative manner are also given in Figure 5.

Figure 5. HRTEM micrographs and FFT analyses **a** -1 wt. %, **b**- 2.5 wt. % and **c**- 5 wt. % Ag

In parallel with calculated crystal size listed in Table 2, HRTEM images with higher magnification shows primary crystals around 15-20nm assembled in the forms of secondary particles as reported previously [22]. HRTEM images revealed some fine particles (~ 20 nm) deposited on larger particles as revealed in Fig 5a, which may corresponds to Ag nanoparticles. However, FFT analyses do not confirmed that these periodically structured crystals belong to Ag.

In a general manner, all as- prepared samples exhibited some Moiré-like fringes, due to lattice parameter mismatch, which implies necessity of heat treatment for structure ordering. FFT analyses had a good accuracy with XRD analyses revealing corresponding atomic planes of Y_2O_3 and relatively poor crystal quality. Since USP is a fast process, with high heating and cooling rates, as- prepared samples may have surface defects and poor crystallinity of constituents which is detrimental to photoluminescence efficiency. In order to improve crystal quality and achieve a uniform nanocomposite structure, heat treatment at 1000 ºC was applied to powders.

3.2. Detailed microstructural and crystallographic study on heat treated nanocomposites

Figure 5 reveals the XRD patterns of 2 h heat treated samples with varying Ag amounts. Moreover, Figure 5 b reveals an illustration on Rietveld refinement on 12 hours heat treated sample with 2.5 wt. % Ag. In Table 2 complete refined crystallographic information are listed for all nanocomposites.

Figure 6. XRD diffraction patterns of **a-** 2 hours heat treated powders with various silver content **b-** Rietveld refinement of sample with 2.5 wt. % Ag 12 h heat treated.

Similar to as prepared samples, BCC cubic structure of $((Y_{0.95}Eu_{0.05})_2O_3$was observed in all nanostructures. However, when compared with diffraction patterns of as prepared samples (see Figure 3), relatively well defined peaks with higher intensities can be observed, which reveals increase in crystal quality after heat treatment. Moreover, two most intense peaks of Ag (111) and (222) have been revealed in samples, indicating better crystallization of Ag in nanocomposite system with heat treatment. Unit cell parameters of heat treated samples as represented in Table 2 has not been affected neither from Ag content nor by heat treatment. They were almost the same with the values already discussed in Table 1.

Table 3. Refined structural parameters of heat treated nanocomposites

	No Ag (2 h)	**1 wt. % Ag (2h)**	**2.5 wt. % Ag (2h)**	**2.5 wt. % Ag (12h)**	**5 wt. % Ag (2h)**
Unit cell parameter *a* (Å)	10.6202	10.6199(2)	10.6199(2)	10.6209(2)	10.6195(2)
Crystallite size (nm)	28.1(3)	42.2(7)	42.1(9)	39.0(5)	42.1(6)
OccY1 (C2)*	0.947	0.936	0.933	0.939	0.945
OccY2 (S6)*	0.939	0.972	0.981	0.963	0.945
R_{Bragg}	1.08	1.083	1.624	1.299	1.552
GoF	1.163	1.345	1.749	1.226	1.168
Rwp	6.759	7.460	4.894	7.269	6.862
Strain	0.169(3)	0.106(2)	0.109(4)	0.101(3)	0.087(3)
Y1:O	2.2301(44)	2.2390(40)	2.2463(54)	2.2270(42)	2.2397(48)
Y2:O	2.2813(45	2.2789(41)	2.2662(54)	2.2810(42)	2.2824(49)

Here, it is necessary to mention that, all samples exhibited increased crystal size with respect to as prepared sample, owing to extra heat energy and longer time provided to system which result in increase in grain boundary mobility and bigger crystal sizes. Similarly, strain values decreased with heat treatment, due to better location of crystals, as reported previously [22]. However, it was observed that samples including silver exhibited more significant crystal growth. Through heat treatment at 1000 °C, since melting point of Ag achieved, liquid Ag exists within Y_2O_3: Eu matrix. As investigated in a previous study, that liquid phase may play crucial a role to be a medium for transporting for the crystal growth, which may end up in bigger crystal size [23]. XRD diffractogram and refined analyses of 2.5 wt. % Ag was also given to reveal the effect of heat treatment time and it was observed that so longer heat treatment times did not yield in a significant improvement superior to 2 hours. Occupancy of Eu has been also affected from heat treatment, C_2 to S_6 band was observed reference and 1 wt. % samples while within 2.5 wt. % and 5 wt. %, S_6 to C_2 shift was revealed. It is worth to highlight that, all these two directions of shifts yield in more homogenous location of Eu^{3+}, which may be promising for luminescence efficiency by increased energy transfer rates.

In order to elucidate the effect of heat treatment on microstructure, samples were also analyzed with HRTEM as represented in Figure 7.

Figure 7. HRTEM/FFT analyses of 2 h heat treated samples **a-** 1 wt . % and **b-** 2.5 wt. % Ag c- 5 wt. % Ag d- 12 h heat treated 2.5wt. % Ag

There was not any sintering tendency *via* heat treatment observed, which is detrimental to luminescence efficiency. Better crystallized and relatively denser morphology was revealed after heat treatment. Especially HRTEM images revealing periodical structures without Moiré fringes as in as prepared powders indicate good crystalline properties, as consistent with XRD findings.

3.3. Formation mechanism of nanocomposites

The process of nanocomposite formation occurs in a dispersed system at the level of few micrometers sized droplets within a very short residence time (3.3 s) and with extremely high heating and cooling rates (approx

50º/s). In stationary conditions, yttrium nitrate hexahydrate decomposition starts with melting of salt at 50 ºC and followed by the formation of intermediate salt at 82 °C and takes place stepwise *via* following general reaction;

$$4Y(NO_3)_3.6H_2O \rightarrow 2Y_2O_3 + 6N_2O_5 + 24H_2O \quad (1)$$

and completed around 580 ºC. It is worth to note decomposition of $4Y(NO_3)_3.6H_2O$ takes place in melt form [24].

Similarly, europium nitrate pentahydrate also first melts around 40-60 ºC between followed by evaporation of $14H_2O$ and $4HNO_3$ between 78 and 229 °C experience stepwise thermal decomposition *via* reaction 2 , most of the reaction takes place till 400 ºC [25]

$$6\ (EuNO_3)_3.6H_2O \rightarrow 3Eu_2O_3 + 6HNO_3 + 12NO_2 + 3O_2 + 33H_2O \quad (2)$$

Like yttrium nitrate, europium nitrate also experience first melting at similar temperatures followed by thermal decomposition. However in the case of silver nitrate: it stays as solid till 200 ºC, since it melts at 212ºC, where the other are starting to experience thermal decomposition. After the other two almost completes decomposition, silver nitrate consecutively precipitates and decomposes at 444 ºC.

$$AgNO_3 \rightarrow Ag + NO_2 + \tfrac{1}{2}\ O_2 \ (\ 444°\ C) \quad (3)$$

Here it is also worth to mention that, although the experiments were performed in air atmosphere, at the reaction temperature of 800 °C, oxidation of Ag into an oxide is not thermodynamically favorable [26]. These thermochemical data imply that initially yttrium and europium nitrates melt and mixed, and then experience thermal decomposition, precipitation and nucleation simultaneously, which makes structure uniform and homogenous. These liquid phase eases the incorporation of Eu^{3+} into the Y_2O_3 lattice. However, Ag formation presumably takes place not simultaneously but consecutively. Due to its different lattice parameter and consecutive precipitation, silver does not incorporate into the lattice of Y_2O_3 but precipitates either in the volume or surface of the secondary particles depending on its concentration. In such a nanocomposite, where the secondary particle, sizing approximately 500nm has a hierarchical structure and represents an assemblage of the primary nano particles (20-40 nm), silver nanoparticles are distributed mostly among and on the surface of the

primary particles. The results of detailed crystallographic and microscopic analyses indicate the primary nano particles represent a BCC Y_2O_3 matrix uniformly substituted by Eu^{3+} ions thus enabling the silver nano particles, being localized on their surface, may exhibit a plasmon effect on luminescence. The model of nanocomposite formation is summarized in Figure 8.

Figure 8. Formation mechanism of as-prepared and heat treated nanocomposites

The mechanism, given in Fig 8, proposed considering thermochemical and structural characterization results. USP process starts with melting of Y and Eu precursors which provides a homogenous mixture of both constituents. After that they start simultaneously to experience stepwise thermal decomposition reaction to form hierarchical nanostructure. During their thermal decomposition, Ag precursor starts to melt and through the end of Y and Eu nitrate decomposition reactions. Ag nitrate starts to decompose. Since Ag experiences reaction steps after Y and Eu, although the rest of the microstructure is uniform, Ag was not integrated well and agglomerated in as prepared samples (See Fig 2). Furthermore, the similar atomic radii of Y and Eu eases for Eu to incorporate into the Y_2O_3 structure, in contrast, Ag represents an ionic size if 1.26 °A and this is energetically not favorable to cause that much strain in the structure. Moreover, the Rietveld refinement given in Table 1 and 3 showed that by incorporation of Ag , there has not been an obvious change in the cell parameter (a), which also indicates Ag precipitates as metal in the structure but does not occupy Y sites [27]. However for Ag with a larger radii (1.26 A), it is not favorable to Moreover, due to fast heating and cooling rates, there were defects, pores and poor crystal arrangement in as prepared samples. During the heat treatment, enough time for diffusion is provided and better crystallization and slight crystal growth were observed. Moreover, since Ag exists as liquid around 1000 °C, a more homogenous and smooth secondary particles (see Fig 6) were observed with respect to as prepared ones (see Fig 2). Moreover, a significant primary crystal growth of $Eu^{3+}:Y_2O_3$ was observed, which implies that Ag did not hinder mobility of grain boundaries since it exists as liquid.

3.4. Photoluminescence results

Fig 9 reveals excitation spectrum of samples with various silver content and heat treatment conditions. For direct comparison purposes, Fig 7a reveals as prepared samples for all Ag concenetrations, 7b reveals 2 hours heat

treated samples for all Ag concentration. Excitation spectrum reveals two bands at 210 nm and 250 nm which are owing to Y^{3+} O^{2}- excitronic band and Eu^{3+} -O^{2-} charge transfer band; respectively.

Fig 9. Excitation spectra of a- as prepared samples b- heat treated samples c

There has been significiant changes obervsed in excitation spectra by silver addition. In as prepared samples, with 1 wt. % Ag addition, there has been a great increase in exitronic band at 210 nm, implying better organized matrix, which is consistent with XRD finding revealing metal induced crystallinization effect. However, more Ag concentrations resulted in weak excitation bands. Moreover, the second peak corresponding to Eu^{3+} -O^{2-} charge transfer becomes broader with Ag addition and shifts to 230 nm, which originates from charge transfer between Eu^{3+} located at S_6 and O^{2-} as consistent with occupancy values reported in Table 1. Intensity of both bands increase with heat treatment and especially with high Ag including systems. Broader second peaks observed in Fig 9 b indicates more homogenous accomodation of Eu^{3+} and increased energy transfer rates again in great agreement with Rietveld refinement.

The emmission spectra of all samples given in Fig 10.

Fig 10. Emission spectra **a**-as synthesized samples (400-700 nm) **b**- all samples (400-600 nm) **c**- heat treated samples (550-650nm) (excited by 230 nm)

Since hypersensitive $^5D_0 \rightarrow {}^7F_2$electric- dipole transition is affacted mostly from local environmental changes, the effect of Ag and heat treatment on that band are mainly investigated in a comparative manner-Typical emmision spectra owing to Eu^3+ transitions between 560-660 nm were observed for all samples. The most intense emmision peak resulting in red light emmission located at 612 nm due to $^5D_0 \rightarrow {}^7F_2$transition of Eu^{3+} ions at C_2position. To compare, emmision peaks in Fig 8b is sharper than ones in Fig 1a, which also proves impovement of crstal quality via heat treatment. Figure 8aalso reveals that thereis a reduction of intensity of that peak with Ag introduction to system, which is in agreement with favoured S_6 occupacyimplied by XRD and excitation behaviour analyses. Addition of Ag changed the local symmetry around Eu^{3+} ions by increasing symmetry as reported in previous

studies [11,13,14]. In parellel, $^5D_0 \rightarrow {}^7F_1$ transitionowingto Eu^{3+} at S_6 sites exhibited stronger intensity in as prepared samples with increasing Ag content as can be seein in Fig 8c. It is also worth to emphasize that only in as prepared samples there has been peaks at ~475 nm detected which corresponds to blue shiftof silver nanoparticles [28]. It was reported that size and distribution of Ag nanoparticles has great importance for enhancement of luminesence. In orderto increase absorption and emmision of matrix by surface plasmons, they need to have a certain distance to emmiter. If there could not been homogenous distribution of emitter (Eu^{3+}) and Ag achieved, than excited dipole may result in energy transfer to the metal and excite the Ag nanoparticles plasmon and quench the emission [29].

2 hours heat treated samples given in Fig 10b exhibits a great increase in emmision instenty, in order to provide a comparison, 2.5 wt. % Ag is also included in that figure to emphasize enhancement. However, further heat treatment (12 hours) was not resulted in any significant change. Therefore, 2 hours heat treatment seems more optimal in terms of PL efficiency and also economical issues. In contrast to as prepared samples, there has been an increase in emmission intensity observed with higher Ag concentration after heat treatment, as well as there has not been any additional peak at 475 nm was detected. This highlighs the uniform distribution of Ag nanoparticles through $Y_{0.95}Eu_{0.05})_2O_3$. Figure 11 represents the CIE diagram of all nanocomposites revealing the color function of the emitted light.

Fig 11. Comparative CIE diagram of phosphors with various synthesis conditions

Among as prepared samples, nanocomposite with 1 wt. % Ag exhibited orange-red colour coordinate while in the case of 2.5 and 5 wt. %, there has been no red emission observed. Moreover, sample with 5 wt. % Ag was almost in blue light region, consistent with emission spectra revealing a peak at 475 nm corresponding to excited Ag plasmons. It is possible to observe that, color coordinates of all heat treated samples independent from Ag content in red light emitting region and close to ideal red chromacity (0.67, 0.33) [30]. These findings are in parallel with structural and photoluminescence analyses; and highlights the efficient red light emission within heat treated samples.

Conclusions

Synthesis of down converting Ag@$(Y_{0.95}\,Eu_{0.05})_2O_3$ phosphors have been performed with USP. Due to the fast nature of USP;e.g. fast heating rates and shorter reaction times, the heat treatment following synthesis is highly required to provide unfirom distribution of constituents. Higher Ag concentrations of as prepared samples resulted in emmission quenching and yielded in poor luminesence. However, Ag enhanced emmision was observed within heat treated samples. 2.5 wt. % Ag incorporation followed by 2 hours heat tratment at 1000°C is reported as the most promising red light emitting phosphor synthesis conditions via USP.

Acknowledgements:

Authors would like to acknowledge projects OI172035 and III45020, Ministry for Education, Science and Technological Development of Serbia Authors would like to thank Friedrich Rosen and Vijenthan Sojentham for their support in laboratory**.**

References

[1] K. Marinkovic , L. Mancic , L.S. Gomez , M.E. Rabanal , M. Dramicanin , O. Milosevic, Photoluminescent properties of nanostructured Y2O3:Eu3+ powders obtained through aerosol synthesis, Optical Materials 32 (2010) 1606–1611.

[2] L. S. Gomez, K. Marinkovic, J. M. Torralba, M. E. Rabanal, O. Milosevic, Nanostructured Y2O3 particles doped with europium synthesized by aerosol route, International Journal of Modern Manufacturing Technologies ISSN 2067–3604, 1(1) (2009).

[3] L.R. Singh, R.S. Ningthoujam, V. Sudarsan, I. Srivastava, S.D. Singh, G.K. Dey, S.K. Kulshreshtha, Luminescence study on Eu3+ doped Y2O3 nanoparticles: particle size, concentration and core–shell formation effects, Nanotechnology 19 (2008) 055201.

[4] Z. Antic, R. Krsmanovic, T. Dramicanin, M. Dramicanin, Optical Properties of Y2O3:Eu3+ Red Emitting Phosphor Obtained via Spray Pyrolysis, Acta Phys. Polonica A116 (2009) 622.

[5] X. Hou, S. Zhou, Y. Li, W. Li, Luminescent properties of nano-sized Y2O3:Eu fabricated by co-precipitation method, J. Alloys Compd. 494 (2010) 382.

[6] Saji Thomas Kochuveedu, Dond Ha Km, Surface plasmon resonance mediated photoluminescence properties of nanostructured multicomponent fluorophore systems, Nanoscale 6 (2014) 4966.

[7] Y.L. Min, Y. Wan, S.H. Yu, Au@Y2O3:Eu3+ rare earth oxide hollow sub-microspheres with encapsulated gold nanoparticles and their optical properties, Solid State Sci. 11 (2009) 96–101.

[8] L. Mancic , M. Nikolic , L. Gomez , M.E. Rabanal , O. Milosevic, Directed growth of nanoarchitected hybrid phosphor particles synthesized at low temperature, Advanced Powder Technology 25 (2014) 1442–1448.

[9]Z. Liu, P.H. Song, R. Qin, G. Pan, X. Bai, Preparation and optical properties of Ag enwrapped Y2O3:Eu3+ nanoparticles in solution and in powders, Solid state Commun. 137 (2006) 199–202.

[10] P. Reineck, D. Gomez, S. H. Ng, M. Karg, T. Bell,P. Mulvaney and U. Bach, Distance and Wavelength Dependent Quenching of Molecular Fluorescence by Au@SiO2 Core–Shell Nanoparticles, ACS Nano 7 (2013) 6636.

[11] H. Nabika, S. Deki, Surface-enhanced luminescence from Eu3+ complex nearby Ag colloids, Eur. Phys. J. D 24 (2003) 369-372.

[12] X. Fang, H. Song, L. Xie, Q. Liu, H- Zhang, X. Bai, B. Dong, Y. Wang, W. Han, Origin of luminescence enhancement and quenching of europium complex in solution phase containing Ag nanoparticles, The Journal of Chemical Physics 131 (2009).

[13]H. Nabika, S. Deki, Enhancing and Quenching Functions of Silver Nanoparticles on the Luminescent Properties of Europium Complex in the Solution Phase, Eur. Phys. J. B 107 (35) (2003)

[14] Y. Wang, J. Zhou, T. Wang, Enhanced luminescence from europium complex owing to surface plasmon resonance of silver nanoparticles, Materials Letters 62 (2008) 1937-1940.

[15] Q. Wang, F- Song, S. Lin, J. Liu, H. Zhao, C. Zhang, C. Ming., E.Y.B. Pun, Polarization-independent dual-band infrared perfect absorber based on a metal-dielectric-metal elliptical nanodisk array , Optics Express 19 (8) (2011).

[16] G. Kaur, R.K. Verma, D.K. Rai, S.B. Rai, Plasmon-enhanced luminescence of Sm complex using silver nanoparticles in Polyvinyl Alcohol, Journal of Luminesence 132 (2012)1683-1687.

[17] J.L. Ferrari, M.A.Cebim , A.M.Pires , M.A.CoutodosSantos , M.R.Davolos, Y2O3:Eu3+ (5 mol%) with Ag nanoparticles prepared by citrate precursor, Journal of Solid State Chemistry 183 (2010) 2110–2115.

[18]L.Muñoz-Fernandeza, G. Alkan, O. Milošević, M.E. Rabanala, B. Friedrich, Synthesis and characterisation of spherical core-shell Ag/ZnO nanocomposites using single and two – steps ultrasonic spray pyrolysis (USP), in press, (2017) https://doi.org/10.1016/j.cattod.2017.11.029

[19] J. Bogovic, S.Stopic, J. Schroeder, B.Friedrich, Nanosized metallic oxide produced by Ultrasonic Spray Pyrolysis, European Metallurgical Conference Proceedings (2011).

[20] Joint Committee on Powder Diffraction Standard, Diffraction Data File, no. 43-1036, 44-0399 and 04-0783. JCPDS International Center for Diffraction Data, Pennsylvania (1991)

[21] S.R.Herd, P.Chaudhari, M.H. Brodsky, Metal contact induced crystallization in films of amorphous silicon and germanium, J. Non-Cryst. Solids 7 (1972) 309.

[22] V. Lojpur, L. Mancic, M.E. Rabanal, M.D. Dramicanin, Z. Tan, T. Hashishin, S. Ohara, O. Milosevic, Structural, morphological and luminescence properties of nanocrystalline up-converting Y1.89Yb0.1Er0.01O3 phosphor particles synthesized through aerosol route, Journal of Alloys and Compounds, 580 (2013) 584–591.

[23] F. Takei, Crystal Growth from Solid Liquid Mixtures, Crystal Growth Mechanism in Atomic Scale) Journal of the Japanese Association for Crystal Growth 18 (3) (1991)381-389

[24] P. Melnikov ,V. A. Nascimento ,L. Z. Z. Consolo , A. F. Silva, Mechanism of thermal decomposition of yttrium nitrate hexahydrate, Y(NO3)3·6H2O and modeling of intermediate oxynitrates, J Therm Anal Calorim (2013) 111:115–119 DOI 10.1007/s10973-012-2236-3

[25] P. Melnikov, I. V. Arkhangelsky, V. A. Nascimento, L. C. S. de Oliveira, A. F. Silva, L. Z. Zanoni, Thermal properties of europium nitrate hexahydrate Eu(NO3)3·6H2O, Therm Anal Calorim (2017) 128:1353–1358, DOI 10.1007/s10973-016-6047-9

[26]M. L. Zheludkevich and others, 'Oxidation of Silver by Atomic Oxygen', *Oxidation of Metals*, 61.1/2 (2004), 39–48 <https://doi.org/10.1023/B>.

[27] Kenneth Barbalace. Periodic Table of Elements - Sorted by Ionic Radius. EnvironmentalChemistry.com. 1995 - 2019. Accessed on-line: 2/25/2019) https://EnvironmentalChemistry.com/yogi/periodic/ionicradius.html

[28] Chris Geddes, Reviews in Fluorescence 6, 2009.

[29] T. Jennings, M. Singh and G. Strouse, Fluorescent Lifetime Quenching near d = 1.5 nm Gold Nanoparticles: Probing NSET Validity, J. Am. Chem. Soc 128 (2006) 5462.

[30] A Kumaresh, R Arun Kumar, N. Ravikumar, U Madhusoodanan, B Spanigrahi, K Marimuthu, M Anruadha, Structural and photoluminescence studies on europium-doped lithium tetraborate (Eu:Li2B4O7) single crystal grown by microtube Czochralski (μT-Cz) technique, Chin. Phys. B, 25 (5) (2016).

Figure 1

Click here to download high resolution image

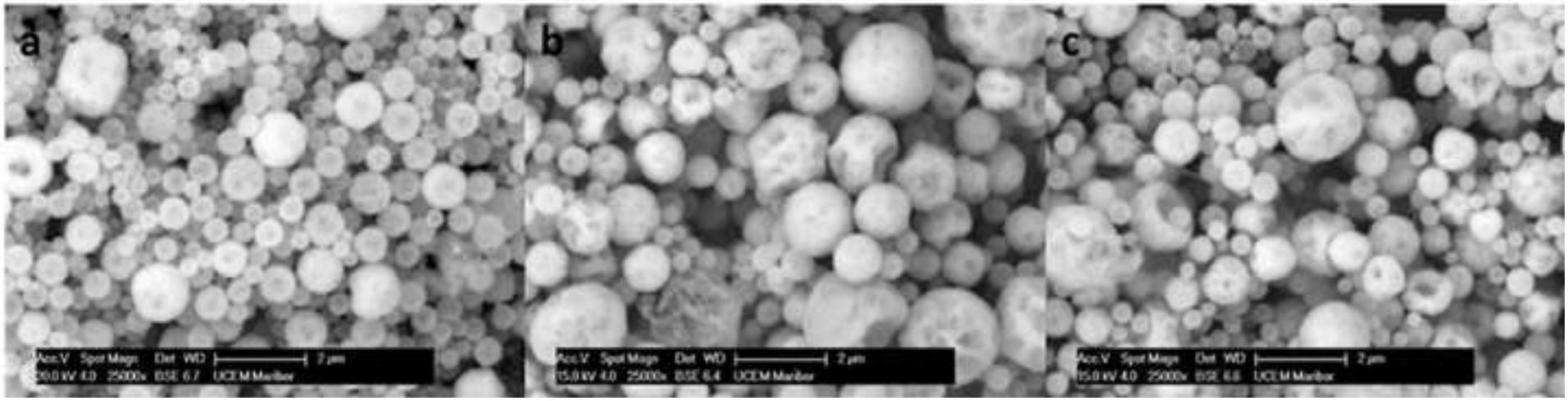

Figure 2

Click here to download high resolution image

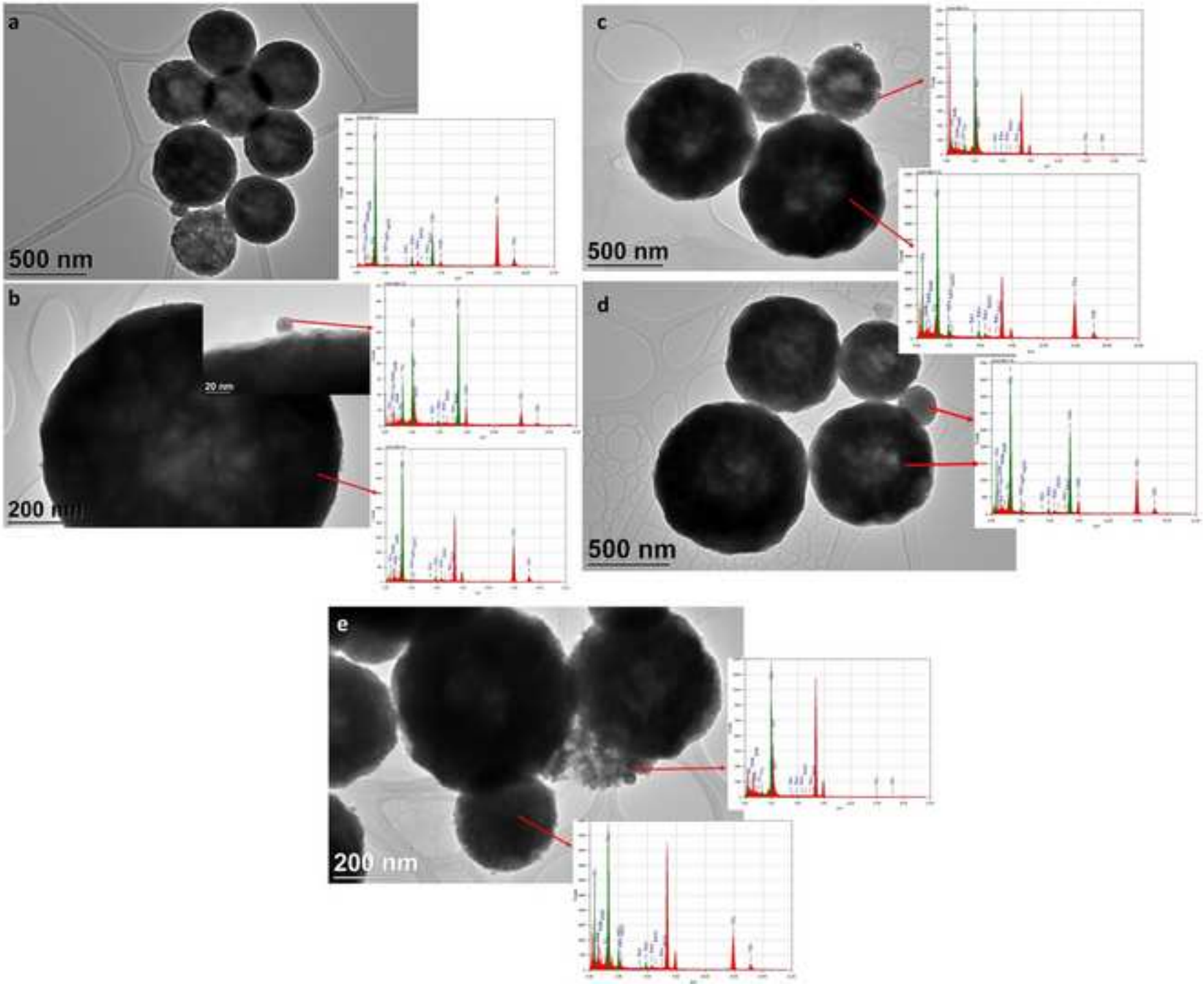

Figure 3

Click here to download high resolution image

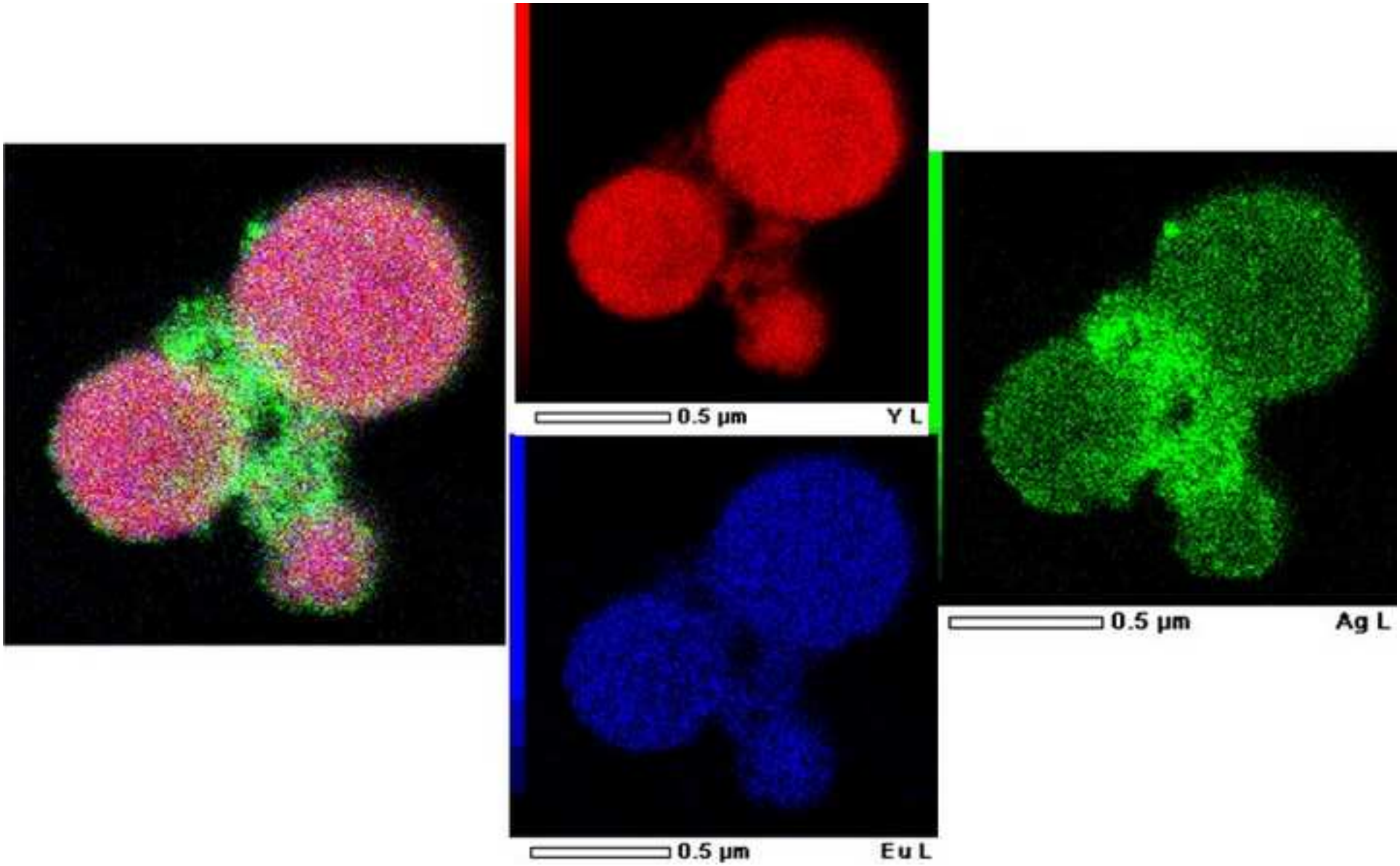

Figure 4

Click here to download high resolution image

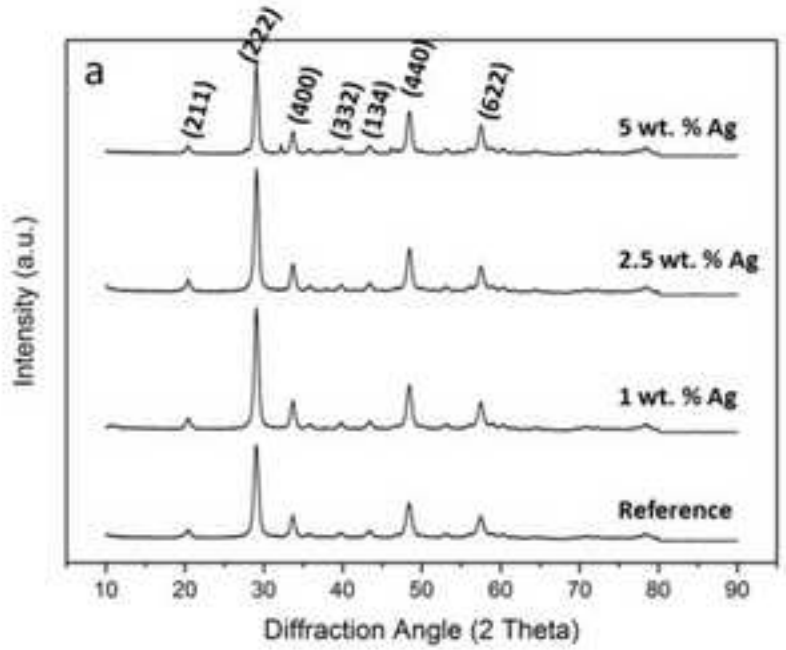

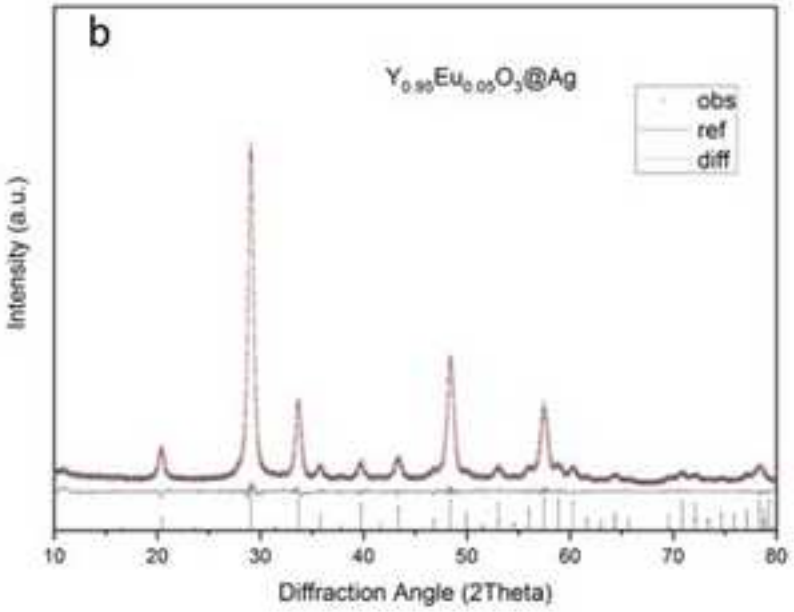

Figure 5

Click here to download high resolution image

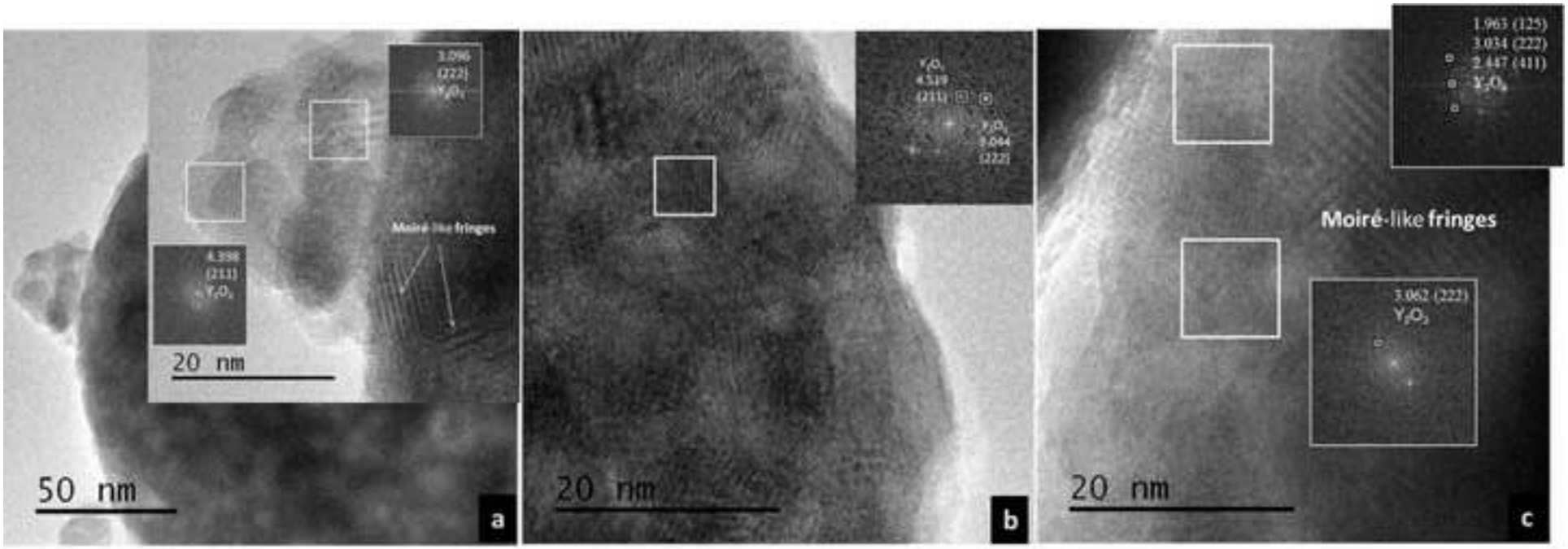

Figure 6

Click here to download high resolution image

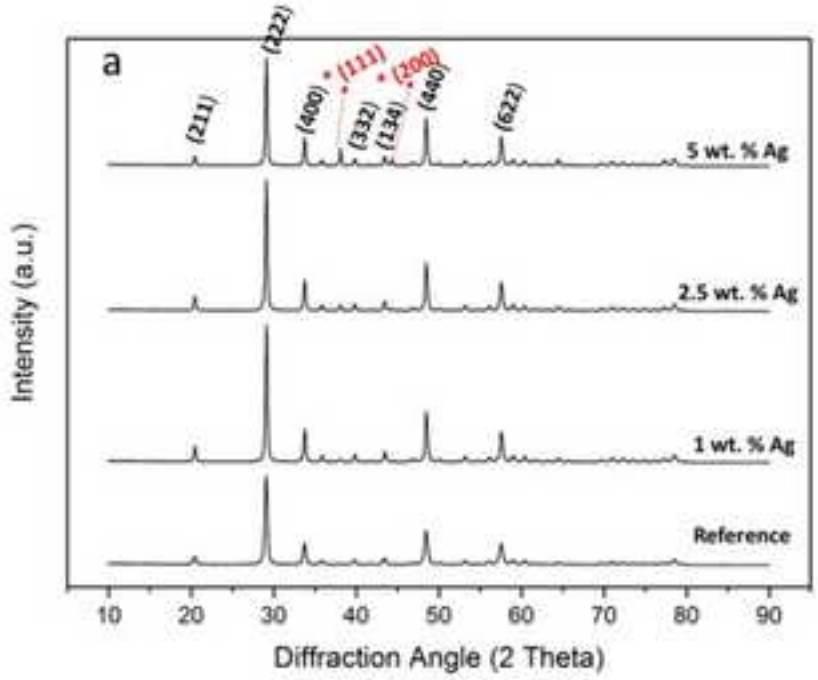

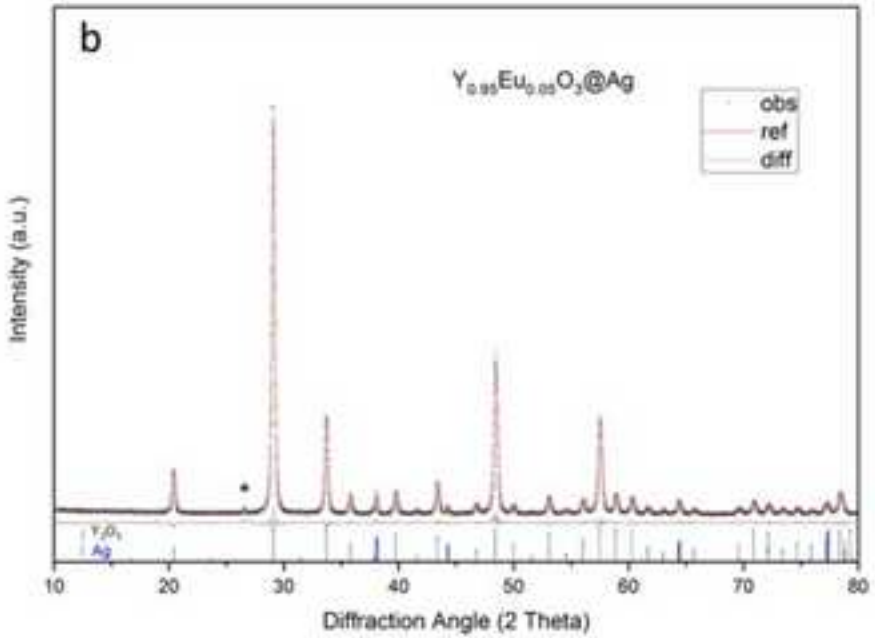

Figure 7

Click here to download high resolution image

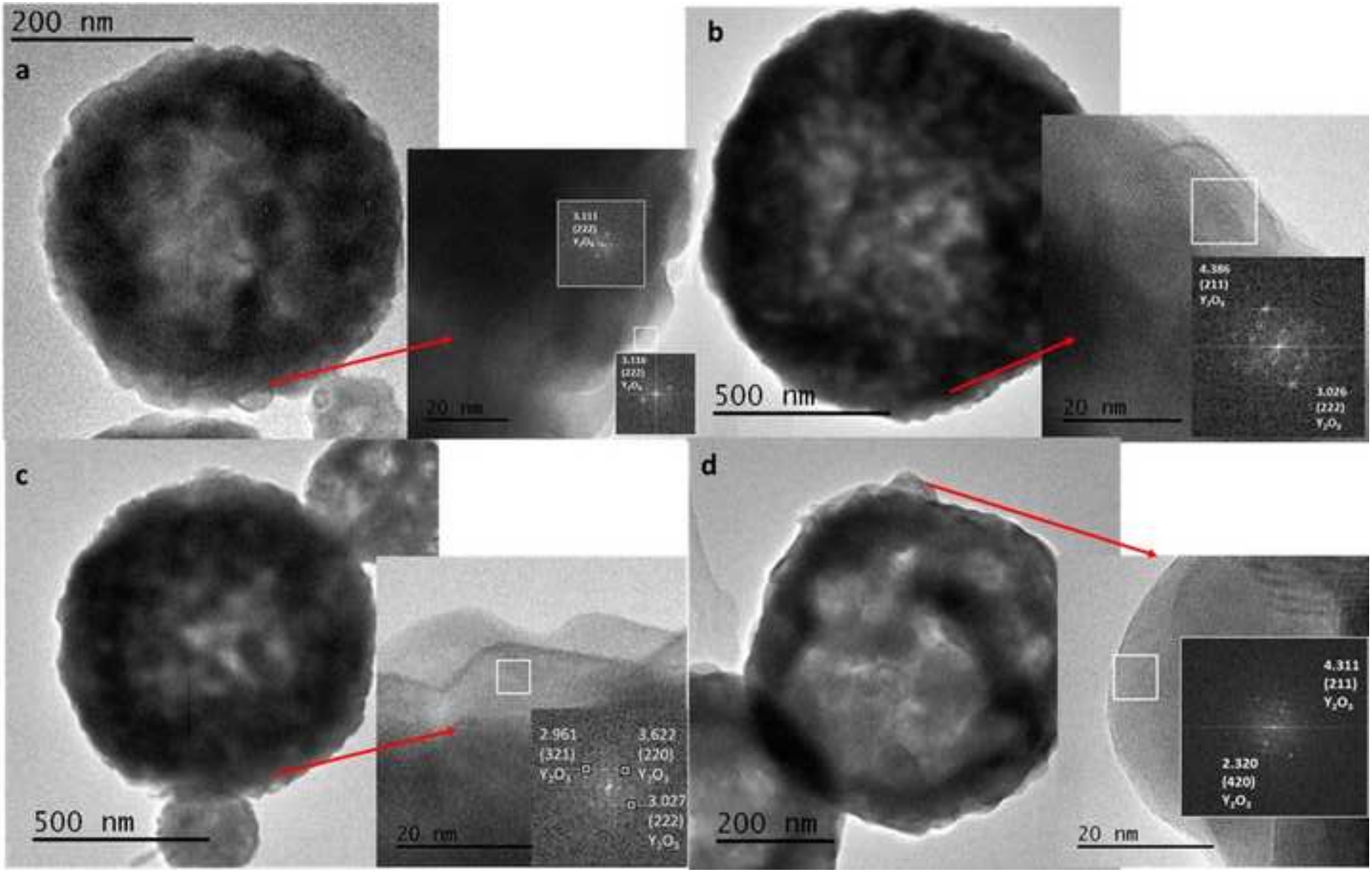

Figure 8

Click here to download high resolution image

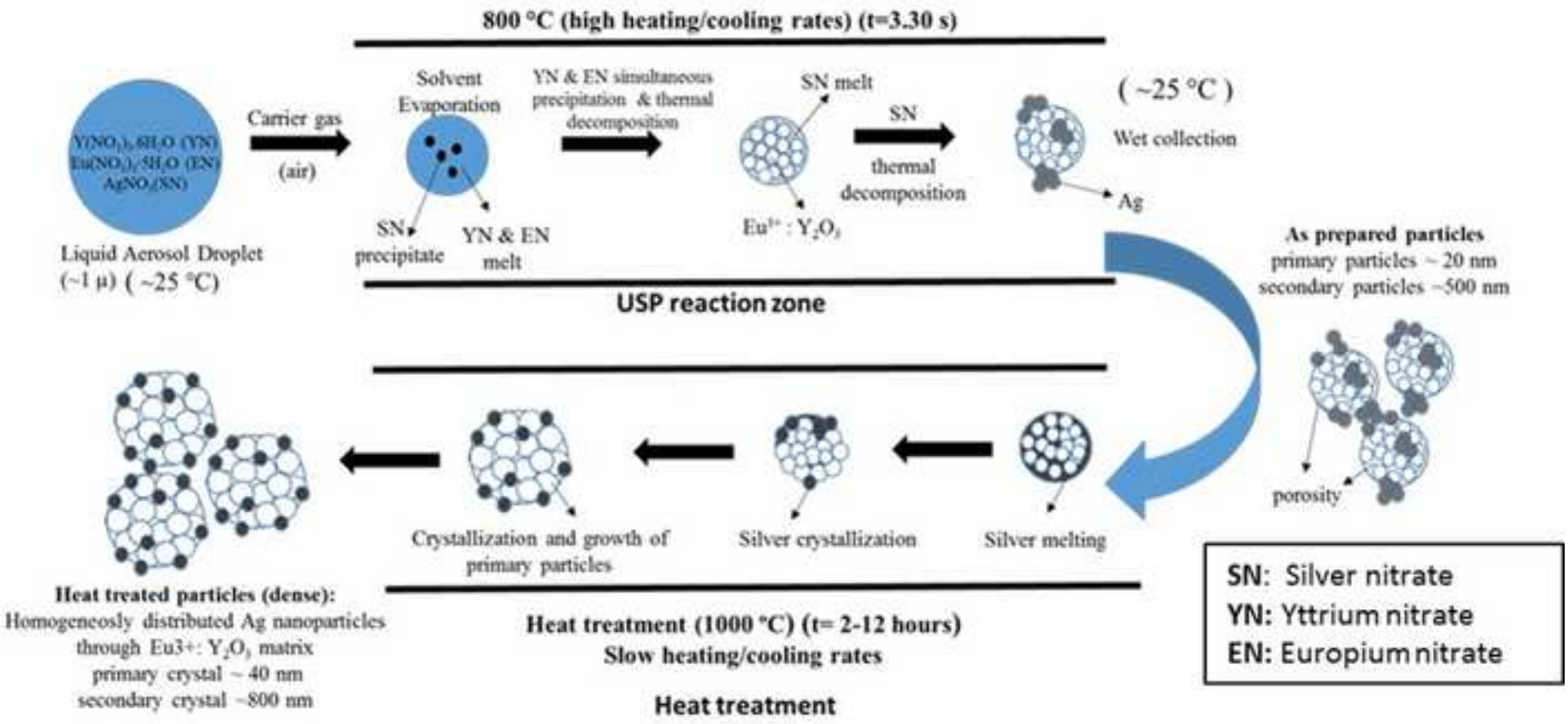

Figure 9

Click here to download high resolution image

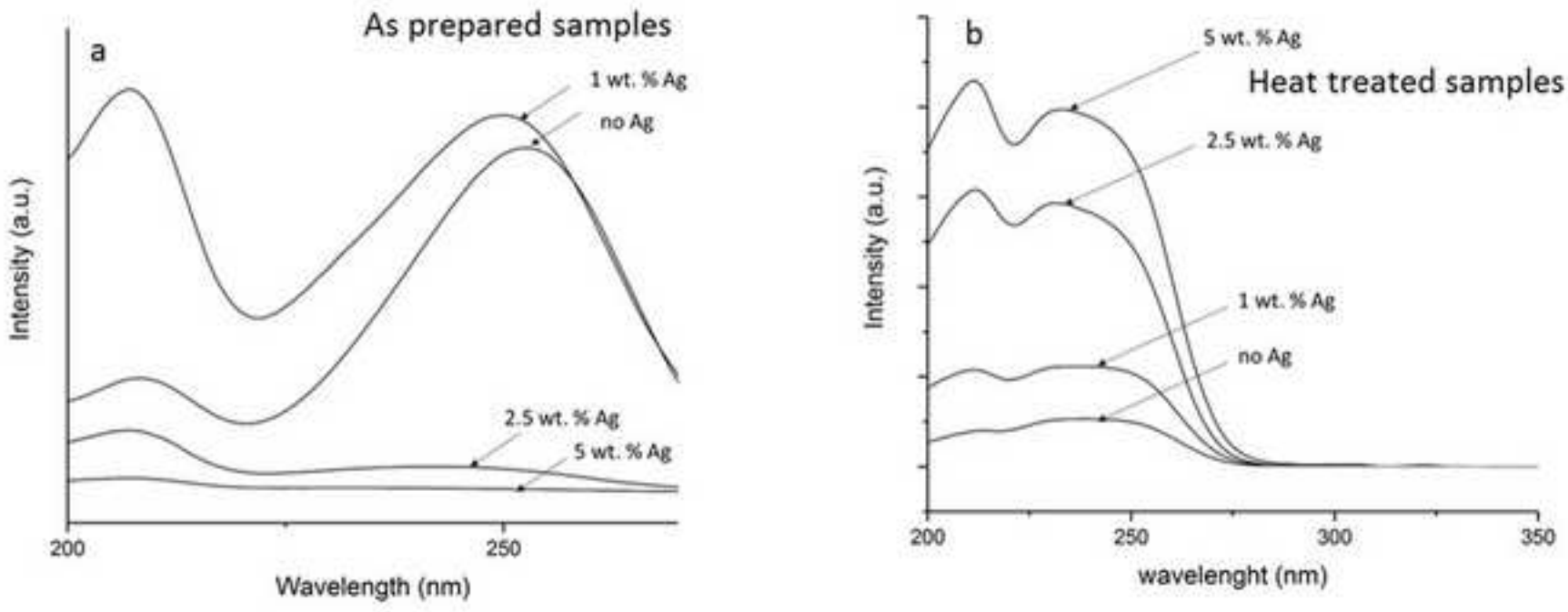

Figure 10

Click here to download high resolution image

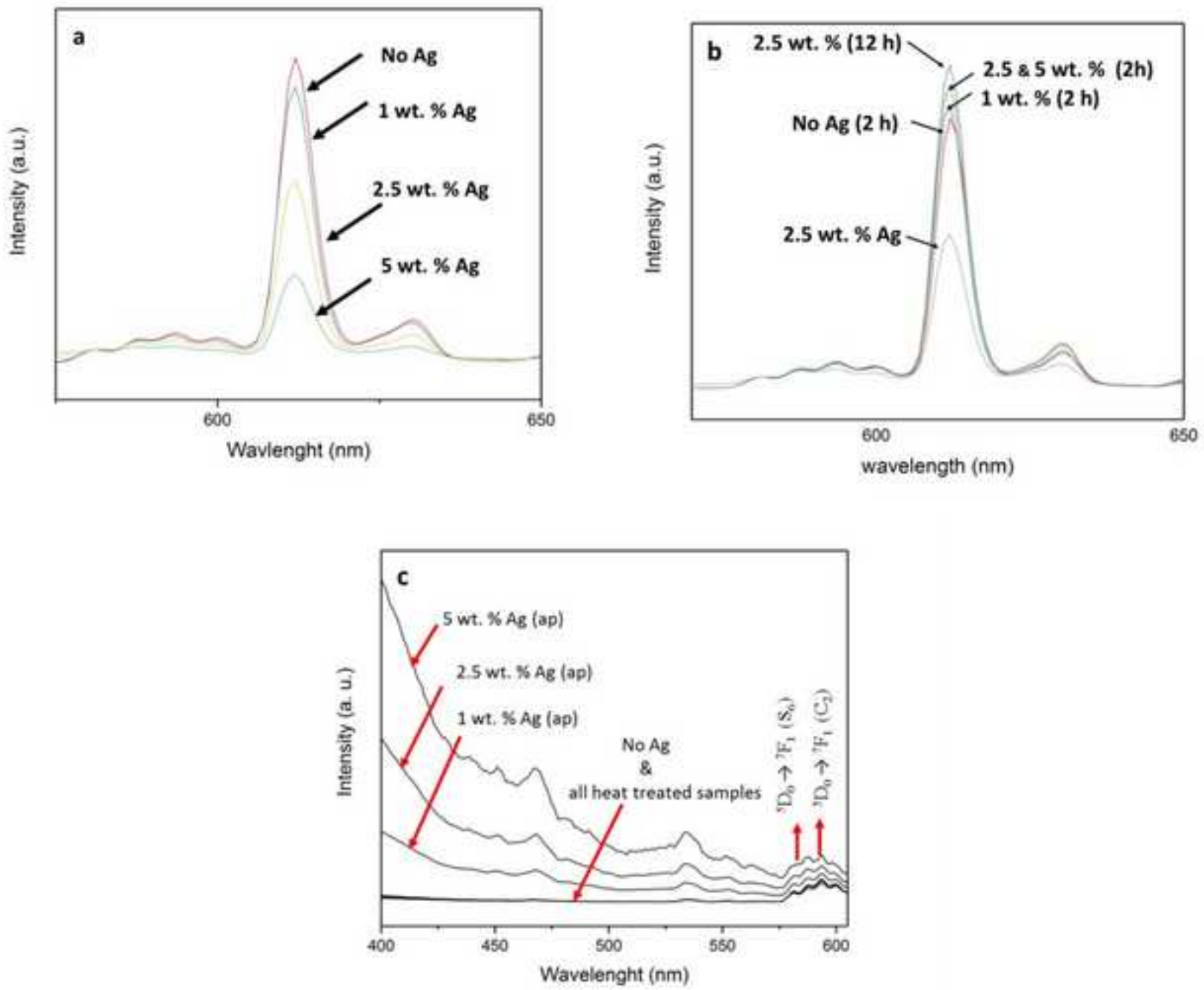

Figure 11

Click here to download high resolution image